Development of Water Soluble Electrospun Fibers for the Oral Delivery of Cannabinoids

Eleftherios G. Andriotis[1,*], Konstantina Chachlioutaki[1], Paraskevi Kyriaki Monou[1], Nikolaos Bouropoulos[2,3], Dimitrios Tzetzis[4], Panagiotis Barmpalexis[1], Ming-Wei Chang[5], Zeeshan Ahmad[6], Dimitrios G. Fatouros[1]

[1]Laboratory of Pharmaceutical Technology, Department of Pharmacy, School of Health Sciences, Aristotle University of Thessaloniki, Thessaloniki GR-54124, Greece

[2]Department of Materials Science, University of Patras, 26504 Rio, Patras, Greece

[3]Foundation for Research and Technology Hellas, Institute of Chemical Engineering and High Temperature Chemical Processes, Patras, Greece

[4]School of Science and Technology, International Hellenic University, Thermi, GR-57001, Greece

[5]Nanotechnology and Integrated Bioengineering Centre, University of Ulster, Jordanstown Campus, Newtownabbey BT37 0QB, Northern Ireland, UK

[6]Leicester School of Pharmacy, De Montfort University, LE1 9BH, Leicester, UK

[*]Corresponding author: Dr. Eleftherios G. Andriotis

e-mail: andrioti@auth.gr

Tel: +302310997653

Fax: +302310997652

Abstract

Cannabidiol and cannabigerol are two active pharmaceutical ingredients, derived from cannabis plant. In the present study, CBD and CBG were co-formulated with polyvinyl(pyrrolidone) (PVP) and Eudragit L-100, using electrohydrodynamic atomization (electrospinning). The produced fibers were smooth and uniform in shape, with average fiber diameters in the range of 700 -900 nm for PVP fibers and 1- 5 μm for Eudragit L-100 fibers. Drug loading and encapsulation efficiency were calculated for all formulations, with high encapsulation efficiencies (over 90%). Both *in vitro* release and *in vitro* disintegration tests of the formulations in SCF and SGF indicated the rapid dissolution of the fibers and the subsequent rapid release of the drugs. The study concluded that the electrospinning process is a fast and efficient method to produce drug-loaded fibers with enhanced properties, suitable for the *per os* administration of cannabinoids.

Keywords: cannabinoids, cannabidiol, cannabigerol, electrospinning, solid dispersion, nanofibers

Introduction

Cannabis and plant-derived cannabinoids have received increasing attention for their potential use for medicinal purposes (1). More than one hundred phytocannabinoids have already been isolated and identified from *Cannabis sativa* (2). Phytocannabinoids are known to interact with the human body *via* the endocannabinoid system, by binding with CB1 or CB2 receptors, resulting in either an agonistic or antagonistic downstream effect (3,4). Due to the wide distribution of these receptors, cannabinoids contribute significantly to human body processes (5,6). One of the most important and most extensively studied cannabinoids, is Δ9-tetrahydrocannabinol (Δ9-THC), mainly due to its psychoactive properties. However, non-psychoactive phytocannabinoids, such as cannabidiol (CBD) and (CBG) have received the attention of the scientific community, as they exhibit similar properties with Δ9-THC. CBD is the most promising of the non-psychoactive cannabinoids due to its pharmacological actions and its abundance in hemp plants (7,8). CBD has been studied for its potential anti-inflammatory activity, antitumoural and anti- angiogenic properties, anti-nausea action, and its ability to alleviate anxiety and pain (9–13). In addition to these, CBD has been asserted of playing a major role in the treatment of various medical conditions, such as multiple sclerosis, Parkinson's disease, Alzheimer's disease, epilepsy, rheumatoid arthritis, and diabetic complications (14–19). Food and Drug Agency (FDA) has already approved the use of CBD for the treatment of seizures associated with Lennox-Gastaut (LGS) or Dravet syndrome (DS) in pediatric patients, and marketed products based on highly purified CBD (Epidiolex®) are already being administered for the treatment of these diseases.

Another interesting phytochemical extracted from *Cannabis sativa,* CBG, plays one of the most significant roles in the biochemistry of the cannabis plant, as it is a chemical precursor to other cannabinoids. Recently, a growing amount of research in

CBG's mechanism of action has revealed its polypharmacological profile, proving its potential health benefits (20). It is suggested that CBG interacts with the two G-protein-coupled receptors, CB1 and CB2, and it is claimed to increase the level of anandamide (the natural ligand of the endocannabinoid receptors), increasing in this way the levels of dopamine, and thus regulating functions such as sleep, mood, and appetite (21). One of the most promising beneficial effects of CBG use is its potential anti-inflammatory, antibacterial, and antidepressant properties (22,23). Additionally, CBG is studied for glaucoma treatment as it contributes to the regulation and lowering of the intraocular pressure (20). Finally, CBG has a positive effect on inhibiting tumor growth in animal models of colorectal cancer (24).

Owing to their low oral bioavailability, efforts have been made towards the development of novel delivery systems *via* different routes of administration, such as transdermal, intranasal, and transmucosal (25,26). Nevertheless, the oral route is the most common due to ease of administration. To this context, a wide range of formulations aimed for oral delivery has been reported including lipid-based delivery systems (SNEDDS), gastro retentive dosage forms, amorphous solid dispersions, and cyclodextrin inclusion complexes (27–31), focusing mainly to cannabinoids solubility enhancement effect.

In this direction, the concept of the development of solid dosage forms to deliver cannabinoids is a persistent challenge. The electrospinning process is considered as one of the most promising drug delivery platforms, aiming to overcome issues related to low dissolution rate (32). Electrospun-based drug delivery systems have flourished in several therapeutic fields due to their unique characteristics, such as flexible pore sizes, high surface area to volume ratio, and ease of production, resulting in ameliorating drug

dissolution and subsequently to enhanced bioavailability of poorly water-soluble active pharmaceutical ingredients (APIs) (32).

The present study is focused on developing, for the first time, electrospun fibers loaded with CBD or CBG (used as model cannabinoids). Two different forms of electrospun fibers based on a nonionic hydrophilic polymer PVP and a pH-responsive polymer (Eudragit-L100), loaded with CBG or CBD, were developed. PVP and Eudragit-L100 were selected as model excipients (matrix-carriers), due to their ability to improve the dissolution profiles when co-formulated with poorly water-soluble APIs, by forming amorphous solid dispersions (ASDs) (33,34). The electrospinning process is one of the most efficient routes for the direct production of ASDs (32,35,36), thus it was selected in this study for the co-formulation of model cannabinoids with two model excipients, towards the improvement of the solubility profiles of both CBD and CBG.

Materials and Methods

Materials

All reagents used were of standard analytical grade. CBD (crystals, > 99% CBD, 1% terpenes by GC-MS, Enecta, Italy; provided by Hempoil®, Athens, Greece) and CBG (crystals, > 99% CBD, 1% terpenes by GC-MS, Enecta, Italy; provided by Hempoil®, Athens, Greece) were used as received with no further purification. All cannabinoids were stored in amber vials purged with nitrogen to ensure an inert atmosphere. PVP (Povidone, average Mw=1,300,000 by LS, Sigma-Aldrich, Darmstadt, Germany) and Eudragit L-100 (Poly(methacrylic acid-co-methyl methacrylate) 1:1, Rohm America, Darmstadt, Germany) were stored in a desiccator at room temperature to avoid any interaction with ambient humidity. All other materials and reagents were of analytical or pharmaceutical grade and were used as received.

Electrospinning Solution Preparation

The electrospinning solutions were prepared according to literature (35,37), with a slight modification. In a typical experiment, 10% w/v and 20% w/v electrospinning solutions were prepared by dissolving the respective polymer (PVP or Eudragit L-100) in ethanol, at room temperature, under magnetic stirring. A predetermined amount of the cannabinoids was added to the polymer solutions and the system was kept under magnetic stirring for at least 30 min before any further processing, to ensure complete dissolution. The different solution compositions are summarized in Table 1.

Dynamic Viscosity Measurements

The dynamic viscosity (μ) of the prepared solutions was measured based on previously reported studies (36). The dynamic viscosity of solutions of 10% w/v PVP and 20% w/v Eudragit L-100 in ethanol was measured using a rotational viscometer (Alpha series, Fungilab, Barcelona, Spain) at 25 °C.

Conductivity Measurements

The electrical conductivity of the polymer solutions was evaluated using a conductivity meter (Fisherbrand™ accumet™ Basic AB30 Conductivity Meter, Fisher Scientific, Loughborough, UK). Briefly, 5mL of each sample was incorporated in a glass tube and the measurement was started by immersing the electrode in the solution. The conductivity value was calculated by the average value of three independent measurements for each sample at ambient temperature.

Electrospinning Process

Electrospun fibers were prepared using an Electrospinning System (Starter Kit, E-Fiber electrospinning system, SKE Research Equipment®, Bollate, Italy). The polymer/drug

148 solutions were transferred in a 2 mL syringe, and the entrapped air was removed. The
149 syringe was fitted with an 18-gauge needle and mounted onto the syringe pump
150 apparatus. The feed rate was set to 1.0 mL/h and 0.5mL/h for PVP and Eudragit-L100
151 solutions, respectively. The applied voltage was constant at 15 ± 2 kV. The distance
152 between the needle tip and the collector was set to 15 cm. All process parameters were
153 selected according to literature (35–38) and to a series of trial experiments. The process
154 was carried out under ambient conditions. The fabricated fiber mats were collected and
155 stored at a desiccator in dark, at room temperature.
156
157 **Scanning Electron Microscopy (SEM)**
158 The morphology of the electrospun samples was studied by a scanning electron
159 microscope (Phenom ProX, ThermoFisher Scientific, Massachusetts, USA) in a high
160 vacuum. Conductive double-sided carbon adhesive tape (TED Pella, Redding,
161 California, USA) was used to mount the samples, which were subsequently coated by
162 gold, using an ion sputtering device (Quorum SC7620, East Sussex, UK). A 15 kV
163 accelerating voltage was applied during the measurements. For fiber diameters
164 distribution calculation, at least 100 measurements per sample were evaluated using the
165 Phenom FiberMetric - Fiber Analysis Software.
166
167 **High-Performance Liquid Chromatography (HPLC)**
168 The quantification of CBD and CBG was performed by high-performance liquid
169 chromatography (HPLC). The system consisted of a pump (LC-10 AD VP), an auto-
170 sampler (SIL-20A HT), and an ultraviolet-visible detector (SPD-10A VP, Shimadzu,
171 Kyoto, Japan). The chromatographic conditions were adapted from the literature, with
172 modifications (30,39). The stationary phase for CBD was a Discovery HS C18 (15 cm

x 4.6 mm, 3 μm) column and the mobile phase consisted of a mixture of (A) acetonitrile and (B) phosphate buffer (KH_2PO_4, 0.0126M, pH 5.0), A:B 80:20. The flow rate was set at 1.0 mL/min and the injection volume was 30 μL. The retention time of CBD and CBG was 5.5 min and 5.0 min, respectively. Standard samples were tested in the range of 0.5-100 μg/mL ($R^2 \geq 0.9999$). Typical chromatograms of CBD and CBG are given as supplementary data (Figure S1 & S2).

Drug Loading

The drug loading and the entrapment efficiency of the samples were measured according to the literature (38). Briefly, the prepared fibers were accurately weighed (10 mg) and dissolved in a mixture of acetonitrile:water 80:20 (1 mL). After complete dissolution, the drug loading and the entrapment efficiency were calculated employing HPLC analysis. The solution concentration was determined using a preconstructed calibration curve of the respective API. The results were presented as the average value of three independent measurements for each sample. CBD and CBG content, along with encapsulation efficiency was expressed according to the following equations:

$$\text{Loading Capacity (\%)} = 100 \times W_{drug}/W_{drug\ loaded\ fiber} \quad (1)$$

where W_{drug} is the weight of the drug in fibrous film and $W_{drug\ loaded\ fiber}$ is the weight of fibrous film sample.

$$\text{Encapsulation Efficiency (\%)} = 100 \times W_{drug}/W_{drug\ used\ in\ the\ formulation} \quad (2)$$

where W_{drug} is the weight of the drug in fibrous film and $W_{drug\ used\ in\ the\ formulation}$ is the initial weight of the drug used in the formulation.

Attenuated Total Reflection Fourier Transformed Infrared (ATR-FTIR) Spectroscopy

The ATR-FTIR spectra were recorded using a Shimadzu IR Prestige-21 spectrometer (Shimadzu, Kyoto, Japan) with a horizontal Golden-Gate MKII single reflection ATR system (Specac, Kent, UK) equipped with ZnSe lenses. In this study, each sample was scanned sixty-four times at 4 cm^{-1} resolution over the wavenumber range of 750–4000 cm^{-1}. The commercially available software IR Solutions (Shimadzu, Japan) was used to process the spectral data.

Thermo-Gravimetric Analysis (TGA)

The thermo-gravimetric analysis was performed by a TGA-50 thermogravimetric analyzer (Shimadzu, Tokyo, Japan). Briefly, 5mg of the samples were heated at a heating rate of 10 °C/min from room temperature to 900°C under nitrogen (flow rate of 50mL/min). All experiments were performed in triplicate.

Differential Scanning Calorimetry (DSC)

DSC analysis was performed by a differential scanning calorimeter 204 F1 Phoenix DSC apparatus (Netsch GmBH, Selb, Germany). Accurately weighted samples were sealed in aluminum pans and heated at a rate of 10°C/min, from 20°C to 120°C under constant nitrogen flow (50 mL/min). The melting point (Tm) of the examined systems was determined as the peak temperature of the heat flow curve, while enthalpy of fusion (ΔHf) was determined as the integrated area in all cases. The standard deviations of temperatures and enthalpies determined in this work were not higher than 1.0 ^{o}C and 3.0 J/g, respectively. The instrument was calibrated for temperature using high purity benzophenone, indium, and tin, while the enthalpic response was calibrated using indium. Thermograms were analyzed using the NETZSCH Proteus – Thermal Analysis

software package version 5.2.1 (NETZSCH, Germany) and all experiments were conducted in triplicate.

Powder X-ray Diffractometry (pXRD)

The crystallinity of the samples was evaluated by XRD analysis, performed by an X-ray diffractometer equipped with a LynxEye type detector (D8-Advance, Bruker, Karlsruhe, Germany). Cu Kα radiation (λ = 0.154059 nm) operated at 40 kV and 40 mA, was used. Data were collected over the 2θ range of 5°-50° at a scanning speed of 0.35 s/step and step size of 0.02°.

***In vitro* Release Studies**

The release of CBD and CBG was studied in Simulated Gastric Fluid (SGF; NaCl, 2 g/L; 1M HCl, 80mL/L; pH 1.2) and in Simulated Intestinal Fluid (SIF; KH_2PO_4, 6.805 g/L; NaOH, 0.896 g/L; pH 6.8). Briefly, release studies for PVP fibers were conducted for 2 h in SGF and SIF, whereas releases studies containing Eudragit L-100 fibers were monitored over a 4 h period equally divided in SGF and SIF, to mimic the transition from gastric to intestinal conditions. All samples were fixed in metal-wire frames (30) to maintain a constant position into the release chamber and they were placed in double-walled glass vessels filled with 40 mL of the release medium, enriched with 0.5% SLS, to ensure sink conditions (30). The experiments were conducted under constant stirring (100 rpm), at 37 °C. Aliquots of 1 mL were withdrawn at specific time intervals, centrifuged at 4500 rcf for 15 min and filtered through 0.45-μm PVDF filters. The samples were analyzed in triplicate by HPLC to determine the concentration of CBD and CBG. Kinetic models were fitted to the release data to investigate the possible release mechanism of the APIs, using DDSolver software (40). The equations 3,4 and

5 describe the first order model, the Korsmeyer-Peppas model and the Peppas-Sahlin model, respectively.

$$dC/dt = K(Cs - C) \quad (3)$$

where C is the concentration of the drug, Cs is the equilibrium solubility at the temperature of the process, K is the first order release constant and t is the time.

$$Mt/M\infty = Kt^n \quad (4)$$

where Mt is the amount of drug released over time t, $M\infty$ is the amount of drug at the equilibrium state, K is the constant and n is the exponent of release and it is related to the release mechanism.

$$Mt/M\infty = K_1t^m + K_2t^{2m} \quad (5)$$

where K_1 and K_2 are constants and m is the Fickian diffusion exponent for a system of any geometrical shape.

***In vitro* Disintegration Test**

The *in vitro* disintegration time was determined according to a Petri dish method, with a slight modification (41,42). A total volume of 2 mL SIF (pH 6.8) or SGF (pH 1.2) was used for the disintegration test. Briefly, the prepared fibrous mats were placed in a glass petri dish and covered with the respective disintegration medium. Time-lapse videos (60 fps) of the procedure were recorded by a digital camera. The test was completed when the fibrous film was disintegrated. The recorded videos were converted to frames and the *in vitro* disintegration time was determined as the time needed for the complete disintegration of the sample.

Water Uptake

To evaluate the water uptake of Eudragit L-100 fiber mats, precisely weighed samples were placed in stainless steel mesh and immersed in two different media, SGF (pH 1.2) and SIF (pH 6.8), respectively. The water uptake of the fibers was monitored for a period of 2 h. At predetermined times intervals, the samples were removed from the apparatus, gently blotted with filter paper to remove excess water, and weighed. The percentage of water uptake was calculated from the following equation:

$$\text{Water uptake (\%)} = (W_2\text{-}W_1)/W_1 \times 100 \quad (6)$$

where W_2 is the weight of the wetted fibers and W_1 is the initial weight of the fibers.

Statistical Analysis

Data were analyzed using Student's t-test. The significance level was set at $p < 0.05$.

Results

Physical Properties of the Spinning Solutions

Viscosity and conductivity measurements were performed for the spinning solutions containing PVP and Eudragit L-100 accordingly. The solution containing 10% w/v PVP had a viscosity of 0.536 ± 0.045 Pa·s, while the viscosity of 20% w/v Eudragit L-100 solution was 0.758 ±0.1 Pa·s (Table 2). The conductivity of PVP and Eudragit L-100 solutions were also measured, and the results are depicted in Table 2.

Electrospun Fibers Morphology

Figure 1 shows the SEM images of the obtained fibers and the respective histograms of fibers' diameters distribution for CBD and CBG loaded nanofibers. The morphology analysis indicates that the applied electrospinning parameters resulted in the production of smooth and uniform fibers. PVP fibers have been successfully produced in

296 cylindrical form while Eudragit L-100 fibers were characterized as flattened (ribbon-
297 like shape). Moreover, the addition of the drugs showed negligible differences with
298 plain solutions.
299
300 **Analysis of CBD and CBG Content**
301 The loading capacity and encapsulation efficiency of all the formulations were
302 calculated as described above. Table 3 lists the values of all the produced fibers
303 containing CBD and CBG. The encapsulation efficiency of both drugs is over 90% and
304 the loading capacity is following the theoretical amount that was initially added in the
305 solution.
306
307 **ATR-FTIR Spectroscopy**
308 The ATR-FTIR spectra of PVP and Eudragit L-100 fibers are shown in Figure 2. The
309 spectrum of Eudragit L-100 reveals bands at 3258 cm^{-1} (-OH), at 2997 cm^{-1} ($-OCH_3$),
310 2952 cm^{-1} ($-CH_3$), and 1731 cm^{-1}(-C=O). The spectrum of PVP reveals bands at 3468
311 cm^{-1} (-OH), at 2955 cm^{-1} (CH_2) , at 2876 cm^{-1} (C-H), at 1657 cm^{-1} (C=O), at 1422 cm^{-1}
312 (C-H), and at 1279 cm^{-1} (C-N) (43). The ATR-FTIR spectra of PVP and Eudragit L-
313 100 fibers indicate the existence of relevant functional groups of PVP and Eudragit L-
314 100. In Figure 2, spectra of pure CBD and CBG are presented, showing two distinct
315 peaks at 1618 cm^{-1} and 1577 cm^{-1}, which are assigned to C=C stretch vibration existing
316 in both CBD and CBG (30). These characteristic peaks of the CBD and CBG are not
317 detected in the ATR-FTIR spectra of the fibers. Additionally, the characteristic peaks
318 of CBD and CBG are also not present in the spectra of physical mixture.
319

TGA Studies

The thermal analysis of the fibers is presented in Figure 3. TGA was applied to investigate the thermal decomposition of fibers. As shown in Figure 3 (A) the thermal degradation of pure CBD and CBG was completed around 250 °C, close to its boiling point, whereas PVP and Eudragit L-100 decompose at a higher temperature (450 °C). Figure 3 (B), (C) presents the recorded TGA thermograms of CBD-loaded fibers, two significant mass losses can be observed from room temperature to 100 °C and from 200 °C until 300 °C, for drug-loaded fibers. The first mass loss, occurring from 70 °C to 100 °C is attributed to water loss. The second mass loss of fibers, starting at 200°C is due to thermal degradation of the polymer matrix and drug. Similarly, the thermal stability of CBG-loaded fibers shows a similar pattern (Figure 3 (D), (E)). Specifically, fibers revealed a weight loss around 100 °C, corresponding to moisture evaporation. The second event occurring at around 250°C is characteristic of the thermal degradation of the CBG.

DSC studies

The DSC thermograms are presented in Figure 4. In regards to the pure APIs the characteristic sharp endothermic peaks for both CBD and CBG, located at 68°C and 52°C, respectively, are attributed to the melting point of the two drugs (44). Additionally, the DSC curves of the drug-loaded fibers exhibited only a wide endotherm around 100 ^{o}C, corresponding to moisture evaporation, with no signs of APIs' melting, indicating that both drugs are probably amorphously dispersed within the prepared fibers matrices. In the case of Eudragit-L100, this hypothesis is verified by the DSC thermograms of the corresponding physical mixtures (Figure 4 (B), (D)), where the melting endotherms of the crystalline APIs are clearly depicted. The absence

of the API endothermic peaks in the case of PVP physical mixtures (Figure 4 (A), (C)) may be attributed to drugs' DSC *in-situ* amorphization. Hence, to verify the amorphization of both drugs within the tested fiber mats, the physical state of both components was also evaluated *via* pXRD analysis.

pXRD Analysis

Figure 5 shows the pXRD patterns of the analyzed samples. As shown in Figure 5 (A) and (B), pure CBD is crystalline with a characteristic peak at 2θ = 9.8, 17.3, and 21.4°. Additionally, characteristic peaks of pure CBG are visible in Figure 5 (C) and (D) at 15.2, 20.8, and 23.9°. Nevertheless, regarding drug-loaded PVP fibers and drug-loaded Eudragit-L100 fibers, no signs of the peaks were observed justifying the amorphous state of the drugs encapsulated into the fibers.

***In vitro* Release Studies**

The *in vitro* release profile of all the formulations is presented in Figures 6 and 7. PVP fibers dissolve within 1 h in both SGF and SIF media, whereas Eudragit-L100 fibers dissolve only in SIF within 2 h. In detail, Figure 6 (A) and 6 (B) depicts the release of CBD from the PVP fibers in SGF and SIF respectively. Complete dissolution of the fibers in the SGF medium, within the first 20 to 30 min, results in a 100% release of CBD, while 2PVP release the drug within 40 min. 1PVP and 2PVP release the drug within 30 min while 3PVP reaches the 100% release within 40 min. In regards, to drug release kinetics, the release profile of 1PVP and 3PVP in SGF medium and 1PVP and 2PVP in SIF medium follow the Korsmeyer-Peppas model (R^2 = 0.9673 and 0.9916, respectively; $n < 0.5$) whereas the release data from 2PVP in SGF medium and 3PVP in SIF medium follow a first-order model (R^2= 0.9947, 0.9776, respectively).

370 Figure 6 (C) depicts the release behavior of CBD from the Eudragit fibers. As evident,
371 CBD release is up to 10% in SGF and as the fibers dissolve in SIF, CBD is completely
372 released. Release kinetics showed that 7EUDR, 8EUDR, and 9EUDR fibers in the SIF
373 medium follow the Peppas-Sahlin model (R^2 = 0.9674, 0.9272, 0.9674, respectively; m
374 < 0.5).
375 Figure 7 presents the release profile of CBG. All formulations have a rapid release
376 within 30 min, while 6PVP releases the drug in a more controlled way. CBG was
377 released from PVP fibers in SIF (Figure 7 (B)), within 20 min. The Korsmeyer-Peppas
378 model was fitted to 4PVP and 5PVP fibers (R^2 = 0.9874, 0.9272, respectively, n < 0.5),
379 and the Peppas-Sahlin model was fitted to 6PVP formulation (R^2 = 0.9593, m < 0.5).
380 All the release data from SIF were fitted to the first-order model (R^2 = 0.9654 - 0.9766).
381 Eudragit fibers release up to 12% of CBG in SGF and complete dissolution of the fibers
382 in SIF release 100% of the API within 2h. The release data from SIF were fitted to the
383 first-order model (R^2 = 0.9123 - 0.9772).
384
385 **Disintegration Test**
386 The disintegration test and wettability studies were carried out by placing 2 cm diameter
387 circular samples of the fibers in SGF and SIF, recording the whole process using a
388 digital camera. The results were presented in Figure 8. Specifically, a complete
389 disintegration of the PVP fibrous structure was occurred in less than 20 sec as evident
390 from Figure 8 (A) & (B). On the contrary Eudragit L-100 fibers showed the expected
391 resistance to dissolution in acidic medium (SGF), whereas they appeared to lose their
392 structure in a moderate rate at neutral pH medium (SIF), resulting in a slow
393 disintegration of the fibers (Figure 8 (C), (D)).
394

Water Uptake

To evaluate the hydration capacity of drug-loaded Eudragit-L100 fibers, swelling studies were performed (Figure 9). The water uptake of Eudragit-L100 fibers in SIF was almost constant for 30 min; then, the samples started to gradually dissolve with an increasing rate.

Discussion

The objective of this study was to investigate the incorporation of cannabinoids into a polymer matrix via the electrospinning process. CBD and CBG loaded fibers were successfully formed by electrospinning technique utilizing PVP and Eudragit L-100 as model matrix carriers.

The SEM images of the produced fibers showed that the prepared solutions resulted in uniform and smooth fibers with a satisfying average diameter. The morphology of the fibers and the absence of beaded fibers, with non-uniform regions is consistent with previous reported studies where electrospun fibers comprised of PVP and Eudragit L-100 (35,37). The formation of ribbon-like shape fibers containing Eudragit L-100 fibers has been previously reported for fibers with diameters in the range of 1-2 μm (45).

The amount of the cannabinoids within the electrospun fibers, was quantified by HPLC analysis. The results are presented in terms of the percentage of loading capacity and encapsulation efficiency of CBD, CBG (Table 3). The high encapsulation efficiency (>90%) is attributed to the electrospinning process, due to rapid solvent evaporation and fast fiber formation (32).

The fabricated fibers along with the pristine materials and their physical mixtures, were analyzed by ATR-FTIR, to investigate the presence of any possible change of the chemical structure of the system during the electrospinning process. The absence of the

420 characteristic peaks of the two cannabinoids from both the fibers and the physical
421 mixtures, is a strong indication that the amount of API within the samples is below the
422 detection limit of the instrument, and thus the deduction of any conclusion regarding
423 the amorphization of the API is not safe.
424 To further investigate the thermophysical properties of the electrospun fibers, TGA
425 analysis was performed. The thermograms are indicative of the hydroscopic nature of
426 both polymers, as there is a mass loss that is attributed to moisture evaporation from
427 the fibers. On the other hand, the mass loss that is observed for all the samples due to
428 APIs' phase change close to their respective boiling points, is an indication that there
429 the thermal properties of the cannabinoids (T_m) have not been altered.
430 The thermophysical properties of the system were further studied by means of DSC
431 analysis. The DSC thermograms of the pure APIs, illustrated the characteristic
432 endothermic peaks of CBD and CBG at 62°C and 58°C, respectively, attributed to their
433 melting point (30,31,44). The absence of these peaks in the drug-loaded fibers implies
434 that the APIs could be in amorphous state (34)**.**
435 To verify the amorphous state of the selected cannabinoids, the pXRD studies were
436 performed to the formatted fibers. pXRD patterns of pure drugs showed characteristic
437 peaks of their crystalline structure (29). On the other hand, the diffractograms of PVP
438 and Eudragit L-100 fibers reveal broad halos typical for amorphous materials (46). The
439 absence of the characteristic peaks of the CBD and CBG from the diffractograms is
440 attributed to the amorphous state of the two substances within the electrospun fibers.
441 The release profiles of the two model cannabinoids from the prepared electrospun fibers
442 were studied *in vitro*. The studies indicated a burst release of CBD and CBG from PVP
443 fibers in SGF and SIF media, whereas both APIs were released from Eudragit L-100
444 fibers in a pH-controlled manner, exhibiting negligible release in lower pH values (SGF

445 medium) and a burst release in the simulated intestinal environment (SIF medium).
446 These observations are consistent with similar systems previously described in the
447 literature (35,46,47), as PVP fibers are readily dissolvable in aqueous media (both SGF
448 and SIF), while Eudragit L-100 fibers are not dissolvable in acidic environment. The
449 release data obtained for the samples 1PVP and 3PVP in SGF and 1PVP and 2PVP in
450 SIF were best fitted to the Korsmeyer-Peppas kinetic model, and based on the 'n' values,
451 it was concluded that the release is governed by Fickian diffusion ($n < 0.5$) (48–50). On
452 the other hand, CBD is released from 2PVP in SGF and 3PVP in SIF medium following
453 the first-order model, indicating that CBD is released in a constant rate between the
454 amount of the drug remaining in the polymer matrix and the released drug (51). In either
455 case, the release of CBD from PVP fibers is mainly affected by the fast dissolution rate
456 of the polymeric fiber, due to the highly hydrophilic nature of PVP (52).
457 The release profiles of CBD from Eudragit L-100 fibers were studied in SIF medium,
458 as the fibers were not dissolved in acidic environment. The release data obtained for
459 the samples 7EUDR, 8EUDR, and 9EUDR in SIF were fitted to the Peppas-Sahlin
460 model ($R^2 = 0.9674, 0.9272, 0.9674$, respectively; $m < 0.5$), indicating that the release
461 of the API is owed to diffusion and relaxation of the polymeric chains (53), attributed
462 to the time-dependent swelling of the polymer, in SIF medium (35,46).
463 The *in vitro* release studies of CBG-containing electrosun fibers, were in close
464 agreement with those obtained for CBD. All formulations exhibited a rapid release
465 within 30 min, with the exception of 6PVP where drug release was slower. The
466 Korsmeyer-Peppas model was fitted to samples 4PVP and 5PVP ($R^2 = 0.9874, 0.9272$,
467 respectively, $n < 0.5$), and the Peppas-Sahlin model was best-fitted to sample 6PVP (R^2
468 $= 0.9593$, $m < 0.5$). All the release data obtained for SIF medium, were fitted to the
469 first-order model ($R^2 = 0.9654 - 0.9766$). In a similar way to CBD release from drug-

loaded PVP fibers, the phenomenon is governed mainly by the fast dissolution of the polymer (as it is described by the Korsmeyer-Peppas model), with the exception of the sample 6PVP, where the swelling of the polymer seems to play a minor role, indicating the presence of drug-polymer interaction of a low extent.

Eudragit fibers released up to 12% of CBG in SGF and complete dissolution of the fibers in SIF release 100% of the API within 2h. The release data from SIF were fitted to the first-order model (R^2 = 0.9123 - 0.9772), indicating the fast dissolution rate of the polymer in SIF medium.

To visualize the fast dissolution rates of both polymers in the studied media, the *in vitro* disintegration test was applied to the electrospun fibers (42). Drug-loaded PVP fibers were completely wetted and disintegrated in both simulated fluids (SGF, SIF) losing their original shape within 20 s, as illustrated in Figure 8 (A) and (B). This rapid disintegration of drug-loaded PVP fibers in both simulated fluids might be attributed to the highly porous structure of the produced fibers during the electrospinning process (55). The porosity of fibers is related to their ability to absorb large quantities of water causing their disintegration in a few seconds. Hence, it can be deduced that the rapid disintegration of fiber structure allowed at the same time the fast release of the drug from the polymer matrix (47).

The disintegration time of drug-loaded Eudragit L-100 fiber mats could not be precisely determined due to the controlled dissolution of the polymer matrix. Hence, the results obtained from the time-lapsed videos (Figure 8 (C), (D)) show a wetting behavior of the fiber mats in SIF until 300 sec with a time-dependent erosion in the polymer matrix. On the contrary, drug-loaded Eudragit fibers are insoluble in acidic pH (SGF pH 1.2) as shown in Figure 8 (C), (D). To this context, the rate and the extent of Eudragit L-100 fibers hydration were investigated at an acidic medium (SGF) and a neutral pH

medium (SIF), to monitor and mimic the transition from gastric to intestinal environment (30). The maximum water uptake was achieved within the first 20 min in both simulated fluids with the the polymer matrix preserving its structure in the acidic medium, whereas a complete disintegration of the fiber structure was observed in SIF medium at the timescale of 2h in pH = 6.8.

Conclusions

To our best knowledge this the first report where electrospinning process was successfully applied to produce submicron fibers containing the model cannabinoids CBD and CBG accordingly. The incorporation of the two poorly water-soluble APIs in two different model excipients (PVP and Eudragit L-100) has led to the increase of CBD's and CBG's solubility, rendering this manufacturing approach suitable for the preparation of water-soluble formulations for *per os* administration of cannabinoids.

References

1. Deiana S, Watanabe A, Yamasaki Y, Amada N, Arthur M, Fleming S, et al. Plasma and brain pharmacokinetic profile of cannabidiol (CBD), cannabidivarine (CBDV), Δ9-tetrahydrocannabivarin (THCV) and cannabigerol (CBG) in rats and mice following oral and intraperitoneal administration and CBD action on obsessive–compulsive behaviour. Psychopharmacology. 2012 Feb;219(3):859–73.
2. ElSohly MA, Slade D. Chemical constituents of marijuana: The complex mixture of natural cannabinoids. Life Sciences. 2005 Dec;78(5):539–48.
3. Pacher P, Bátkai S, Kunos G. The Endocannabinoid System as an Emerging Target of Pharmacotherapy. Pharmacol Rev. 2006 Sep;58(3):389–462.

4. Wassmann CS, Højrup P, Klitgaard JK. Cannabidiol is an effective helper compound in combination with bacitracin to kill Gram-positive bacteria. Sci Rep. 2020 Dec;10(1):4112.
5. Kraft B. Is There Any Clinically Relevant Cannabinoid-Induced Analgesia. Pharmacology. 2012;89(5–6):237–46.
6. Guindon J, Hohmann AG. The endocannabinoid system and pain. CNS Neurol Disord Drug Targets. 2009 Dec;8(6):403–21.
7. Premoli M, Aria F, Bonini SA, Maccarinelli G, Gianoncelli A, Pina SD, et al. Cannabidiol: Recent advances and new insights for neuropsychiatric disorders treatment. Life Sciences. 2019 May;224:120–7.
8. Zuardi AW. Cannabidiol: from an inactive cannabinoid to a drug with wide spectrum of action. Rev Bras Psiquiatr. 2008 Sep;30(3):271–80.
9. Pisanti S, Malfitano AM, Ciaglia E, Lamberti A, Ranieri R, Cuomo G, et al. Cannabidiol: State of the art and new challenges for therapeutic applications. Pharmacology & Therapeutics. 2017 Jul;175:133–50.
10. Romano B, Borrelli F, Pagano E, Cascio MG, Pertwee RG, Izzo AA. Inhibition of colon carcinogenesis by a standardized Cannabis sativa extract with high content of cannabidiol. Phytomedicine. 2014 Apr;21(5):631–9.
11. Parker LA, Mechoulam R, Schlievert C. Cannabidiol, a non-psychoactive component of cannabis and its synthetic dimethylheptyl homolog suppress nausea in an experimental model with rats: Neuroreport. 2002 Apr;13(5):567–70.
12. Boychuk DG, Goddard G, Mauro G, Orellana MF. The Effectiveness of Cannabinoids in the Management of Chronic Nonmalignant Neuropathic Pain: A Systematic Review. J Oral Facial Pain Headache. 2015 Jan;29(1):7–14.

13. Solinas M, Massi P, Cantelmo A, Cattaneo M, Cammarota R, Bartolini D, et al. Cannabidiol inhibits angiogenesis by multiple mechanisms: Cannabidiol and angiogenesis. British Journal of Pharmacology. 2012 Nov;167(6):1218–31.
14. Rudroff T, Sosnoff J. Cannabidiol to Improve Mobility in People with Multiple Sclerosis. Frontiers in Neurology. 2018;9:183.
15. More SV, Choi D-K. Promising cannabinoid-based therapies for Parkinson's disease: motor symptoms to neuroprotection. Mol Neurodegener. 2015 Apr 8;10:17.
16. Aso E, Ferrer I. Cannabinoids for treatment of Alzheimer's disease: moving toward the clinic. Front Pharmacol [Internet]. 2014 Mar 5 [cited 2020 Oct 1];5
17. Silvestro S, Mammana S, Cavalli E, Bramanti P, Mazzon E. Use of Cannabidiol in the Treatment of Epilepsy: Efficacy and Security in Clinical Trials. Molecules. 2019 Apr 12;24(8):1459.
18. Malfait AM, Gallily R, Sumariwalla PF, Malik AS, Andreakos E, Mechoulam R, et al. The nonpsychoactive cannabis constituent cannabidiol is an oral anti-arthritic therapeutic in murine collagen-induced arthritis. Proceedings of the National Academy of Sciences. 2000 Aug 15;97(17):9561–6.
19. Noreen N, Muhammad F, Akhtar B, Azam F, Anwar MI. Is Cannabidiol a Promising Substance for New Drug Development? A Review of its Potential Therapeutic Applications. Crit Rev Eukaryot Gene Expr. 2018;28(1):73–86.
20. Deiana S. Potential Medical Uses of Cannabigerol: A Brief Overview. In: Handbook of Cannabis and Related Pathologies [Internet]. Elsevier; 2017 [cited 2020 Oct 1]. p. 958–67.

21. Brierley DI, Samuels J, Duncan M, Whalley BJ, Williams CM. Cannabigerol is a novel, well-tolerated appetite stimulant in pre-satiated rats. Psychopharmacology. 2016 Oct;233(19–20):3603–13.

22. Borrelli F, Fasolino I, Romano B, Capasso R, Maiello F, Coppola D, et al. Beneficial effect of the non-psychotropic plant cannabinoid cannabigerol on experimental inflammatory bowel disease. Biochemical Pharmacology. 2013 May;85(9):1306–16.

23. Appendino G, Gibbons S, Giana A, Pagani A, Grassi G, Stavri M, et al. Antibacterial Cannabinoids from Cannabis sativa: A Structure-Activity Study. J Nat Prod. 2008 Aug;71(8):1427–30.

24. Borrelli F, Pagano E, Romano B, Panzera S, Maiello F, Coppola D, et al. Colon carcinogenesis is inhibited by the TRPM8 antagonist cannabigerol, a Cannabis-derived non-psychotropic cannabinoid. Carcinogenesis. 2014 Dec;35(12):2787–97.

25. Paudel KS, Hammell DC, Agu RU, Valiveti S, Stinchcomb AL. Cannabidiol bioavailability after nasal and transdermal application: effect of permeation enhancers. Drug Development and Industrial Pharmacy. 2010 Sep 1;36(9):1088–97.

26. Itin C, Barasch D, Domb AJ, Hoffman A. Prolonged oral transmucosal delivery of highly lipophilic drug cannabidiol. International Journal of Pharmaceutics. 2020 May;581:119276.

27. Izgelov D, Shmoeli E, Domb AJ, Hoffman A. The effect of medium chain and long chain triglycerides incorporated in self-nano emulsifying drug delivery systems on oral absorption of cannabinoids in rats. International Journal of Pharmaceutics. 2020 Apr;580:119201.

592 28. Izgelov D, Freidman M, Hoffman A. Investigation of cannabidiol gastro retentive
593 tablets based on regional absorption of cannabinoids in rats. European Journal of
594 Pharmaceutics and Biopharmaceutics. 2020 Jul;152:229–35.
595 29. Lv P, Zhang D, Guo M, Liu J, Chen X, Guo R, et al. Structural analysis and
596 cytotoxicity of host-guest inclusion complexes of cannabidiol with three native
597 cyclodextrins. Journal of Drug Delivery Science and Technology. 2019
598 Jun;51:337–44.
599 30. Andriotis EG, Monou P-K, Louka A, Papaefstathiou E, Eleftheriadis GK,
600 Fatouros DG. Development of food grade 3D printable ink based on pectin
601 containing cannabidiol/cyclodextrin inclusion complexes. Drug Development and
602 Industrial Pharmacy. 2020;1–9.
603 31. Koch N, Jennotte O, Gasparrini Y, Vandenbroucke F, Lechanteur A, Evrard B.
604 Cannabidiol aqueous solubility enhancement: Comparison of three amorphous
605 formulations strategies using different type of polymers. International Journal of
606 Pharmaceutics. 2020 Nov;589:119812.
607 32. Yu D-G, Li J-J, Williams GR, Zhao M. Electrospun amorphous solid dispersions
608 of poorly water-soluble drugs: A review. Journal of Controlled Release. 2018
609 Dec;292:91–110.
610 33. Monschke M, Wagner KG. Amorphous solid dispersions of weak bases with pH-
611 dependent soluble polymers to overcome limited bioavailability due to gastric pH
612 variability – An in-vitro approach. International Journal of Pharmaceutics. 2019
613 Jun;564:162–70.
614 34. Kapourani A, Chatzitheodoridou M, Kontogiannopoulos KN, Barmpalexis P.
615 Experimental, Thermodynamic, and Molecular Modeling Evaluation of

Amorphous Simvastatin-Poly(vinylpyrrolidone) Solid Dispersions. Mol Pharmaceutics. 2020 Jul 6;17(7):2703–20.

35. Reda R, Wen MM, El-Kamel A. Ketoprofen-loaded Eudragit electrospun nanofibers for the treatment of oral mucositis. IJN. 2017 Mar;Volume 12:2335–51.

36. Ignatova M, Manolova N, Rashkov I. Novel antibacterial fibers of quaternized chitosan and poly(vinyl pyrrolidone) prepared by electrospinning. European Polymer Journal. 2007 Apr;43(4):1112–22.

37. Chuangchote S, Sagawa T, Yoshikawa S. Electrospinning of poly(vinyl pyrrolidone): Effects of solvents on electrospinnability for the fabrication of poly(p-phenylene vinylene) and TiO2 nanofibers. J Appl Polym Sci. 2009 Dec 1;114(5):2777–91.

38. Nazari K, Kontogiannidou E, Haj Ahmad R, Andreadis D, Rasekh M, Bouropoulos N, et al. Fibrous polymeric buccal film formulation, engineering and bio-interface assessment. European Polymer Journal. 2017 Dec;97:147–57.

39. Brighenti V, Pellati F, Steinbach M, Maran D, Benvenuti S. Development of a new extraction technique and HPLC method for the analysis of non-psychoactive cannabinoids in fibre-type Cannabis sativa L. (hemp). Journal of Pharmaceutical and Biomedical Analysis. 2017 Sep;143:228–36.

40. Zhang Y, Huo M, Zhou J, Zou A, Li W, Yao C, et al. DDSolver: An Add-In Program for Modeling and Comparison of Drug Dissolution Profiles. AAPS J. 2010 Sep;12(3):263–71.

41. Garsuch V, Breitkreutz J. Comparative investigations on different polymers for the preparation of fast-dissolving oral films. Journal of Pharmacy and Pharmacology. 2010 Apr;62(4):539–45.

641 42. Chachlioutaki K, Tzimtzimis EK, Tzetzis D, Chang M-W, Ahmad Z, Karavasili
642 C, et al. Electrospun Orodispersible Films of Isoniazid for Pediatric Tuberculosis
643 Treatment. Pharmaceutics. 2020 May 21;12(5):470.
644 43. Huang S, Zhou L, Li M-C, Wu Q, Kojima Y, Zhou D. Preparation and Properties
645 of Electrospun Poly (Vinyl Pyrrolidone)/Cellulose Nanocrystal/Silver
646 Nanoparticle Composite Fibers. Materials. 2016 Jun 28;9(7):523.
647 44. Stinchcomb AL, Valiveti S, Hammell DC, Ramsey DR. Human skin permeation
648 of Delta8-tetrahydrocannabinol, cannabidiol and cannabinol. Journal of Pharmacy
649 and Pharmacology. 2004 Mar;56(3):291–7.
650 45. Koombhongse S, Liu W, Reneker DH. Flat polymer ribbons and other shapes by
651 electrospinning. J Polym Sci B Polym Phys. 2001 Nov 1;39(21):2598–606.
652 46. Illangakoon UE, Yu D-G, Ahmad BS, Chatterton NP, Williams GR. 5-
653 Fluorouracil loaded Eudragit fibers prepared by electrospinning. International
654 Journal of Pharmaceutics. 2015 Nov;495(2):895–902.
655 47. Samprasit W, Akkaramongkolporn P, Ngawhirunpat T, Rojanarata T,
656 Kaomongkolgit R, Opanasopit P. Fast releasing oral electrospun PVP/CD
657 nanofiber mats of taste-masked meloxicam. International Journal of
658 Pharmaceutics. 2015 Jun;487(1–2):213–22.
659 48. Barman M, Mahmood S, Augustine R, Hasan A, Thomas S, Ghosal K. Natural
660 halloysite nanotubes /chitosan based bio-nanocomposite for delivering
661 norfloxacin, an anti-microbial agent in sustained release manner. International
662 Journal of Biological Macromolecules. 2020 Nov;162:1849–61.
663 49. Ghosal K, Adak S, Agatemor C, G P, Kalarikkal N, Thomas S. Novel
664 interpenetrating polymeric network based microbeads for delivery of poorly water
665 soluble drug. J Polym Res. 2020 Apr;27(4):98.

50. Ghosal K, Das A, Das SK, Mahmood S, Ramadan MAM, Thomas S. Synthesis and characterization of interpenetrating polymeric networks based bio-composite alginate film: A well-designed drug delivery platform. International Journal of Biological Macromolecules. 2019 Jun;130:645–54.
51. Ammoury N, Fessi H, Devissaguet JP, Puisieux F, Benita S. In Vitro Release Kinetic Pattern of Indomethacin from Poly(D,L-Lactide) Nanocapsules. Journal of Pharmaceutical Sciences. 1990 Sep;79(9):763–7.
52. Wojcik-Pastuszka D, Krzak J, Macikowski B, Berkowski R, Osiński B, Musiał W. Evaluation of the Release Kinetics of a Pharmacologically Active Substance from Model Intra-Articular Implants Replacing the Cruciate Ligaments of the Knee. Materials. 2019 Apr 12;12(8):1202.
53. Mathematical models of drug release. In: Strategies to Modify the Drug Release from Pharmaceutical Systems [Internet]. Elsevier; 2015 [cited 2020 Oct 1]. p. 63–86.
54. Illangakoon UE, Gill H, Shearman GC, Parhizkar M, Mahalingam S, Chatterton NP, et al. Fast dissolving paracetamol/caffeine nanofibers prepared by electrospinning. International Journal of Pharmaceutics. 2014 Dec;477(1–2):369–79.

Table 1. Different compositions of the spinning solutions.

Sample	Polymer Concentration (% w/v)*	Cannabinoid Concentration (% w/w)**	Type of Cannabinoid
1PVP	10	0.5	CBD
2PVP		1	
3PVP		1.5	
4PVP		0.5	CBG
5PVP		1	
6PVP		1.5	

7EUDR	20	0.5	CBD
8 EUDR		1	
9 EUDR		1.5	
10EUDR		0.5	CBG
11EUDR		1	
12EUDR		1.5	

*Final polymer concentration in ethanol

**Concentration based on the final polymer content

685

686

687

688 **Table 2**. Apparent viscosity and conductivity values of the spinning solutions.

Electrospinning solutions	Viscosity (Pa·s)	Conductivity (μS/cm)
PVP	0.536 ±0.045	67.5 ±0.4
Eudragit L-100	0.758 ±0.1	91.3±0.55

689

690

691

692

693

694

695 **Table 3**. Loading capacity (%) and Encapsulation efficiency (%) of the formulations.

Sample	Loading Capacity (%)	Encapsulation efficiency (%)
1PVP	0.47	93.90
2PVP	0.99	99.00
3PVP	1.48	98.10
4PVP	0.49	98.56
5PVP	0.97	97.10
6PVP	1.46	97.13

7EUDR	0.45	90.50
8EUDR	0.95	95.45
9EUDR	1.48	98.50
10EUDR	0.49	98.88
11EUDR	0.94	93.65
12EUDR	1.42	94.35

696
697
698
699
700
701
702
703
704
705
706
707
708
709
710
711
712
713
714

715 **FIGURE LEGENDS**

716

717 **Figure 1.** SEM images and average diameter distribution histograms of a. CBD loaded
718 PVP fibers (A) PVP, (B) 1PVP, (C) 2PVP, (D) 3PVP, b. CBD loaded Eudragit L-100
719 fibers I Eudragit L-100, (F) 7EUDR, (G) 8EUDR, (H)9EUDR, c. CBG loaded PVP
720 fiber mats (I)PVP, (J)4PVP, (K)5PVP, (L)6PVP, d. CBG loaded Eudragit L-100 fibers
721 (M) Eudragit L-100, (N)10EUDR, (0)11EUDR, (P)12EUDR.

Figure 2. ATR-FTIR spectra of (A) as-spun PVP/CBD fibers and Physical mixtures, (B) as-spun Eudragit L-100/CBD fibers and Physical mixtures, (C) as-spun PVP/CBG fibers and Physical mixtures, (D) as-spun Eudragit L-100/CBG fibers and Physical mixtures.

Figure 3. TGA results of nanofibers: (A) Raw material, (B) as spun PVP/CBD fibers, (C) as spun Eudragit L-100/CBD fibers, (D) as spun PVP/CBG fibers, (E) as spun Eudragit L-100/CBG fibers.

Figure 4. DSC thermograms of nanofibers: (A) PVP/CBD fibers and Physical mixtures, (B) Eudragit L-100/CBD fibers and Physical mixtures, (C) PVP/CBG fibers and Physical mixtures, (D) Eudragit L-100/CBG fibers and physical mixtures.

Figure 5. pXRD pattern of (A) PVP/CBD fibers; (B) Eudragit L-100/CBD fibers, (C) PVP/CBG fibers, (D) Eudragit L-100/CBG fibers.

Figure 6. Release profile of CBD from PVP fibers in (A) SGF and (B) SIF and from Eudragit fibers (C) in SGF and SIF.

Figure 7. Release profile of CBG from PVP fibers in (A) SGF and (B) SIF and from Eudragit fibers (C) in SGF and SIF.

Figure 8. Disintegration test of fiber in Simulated fluids: (A) 3PVP in SGF and SIF, (B) 6PVP in SGF and SIF, (C) 9EUDR in SGF and SIF, (D) 12EUDR in SGF and SIF.

747 **Figure 9.** Swelling plot of drug-loaded Eudragit L-100 fibers: (A) in SGF, (B) in SIF

748
749
750
751
752
753
754
755
756
757
758
759
760
761
762
763
764
765
766
767
768
769
770
771

772 **FIGURE 1**

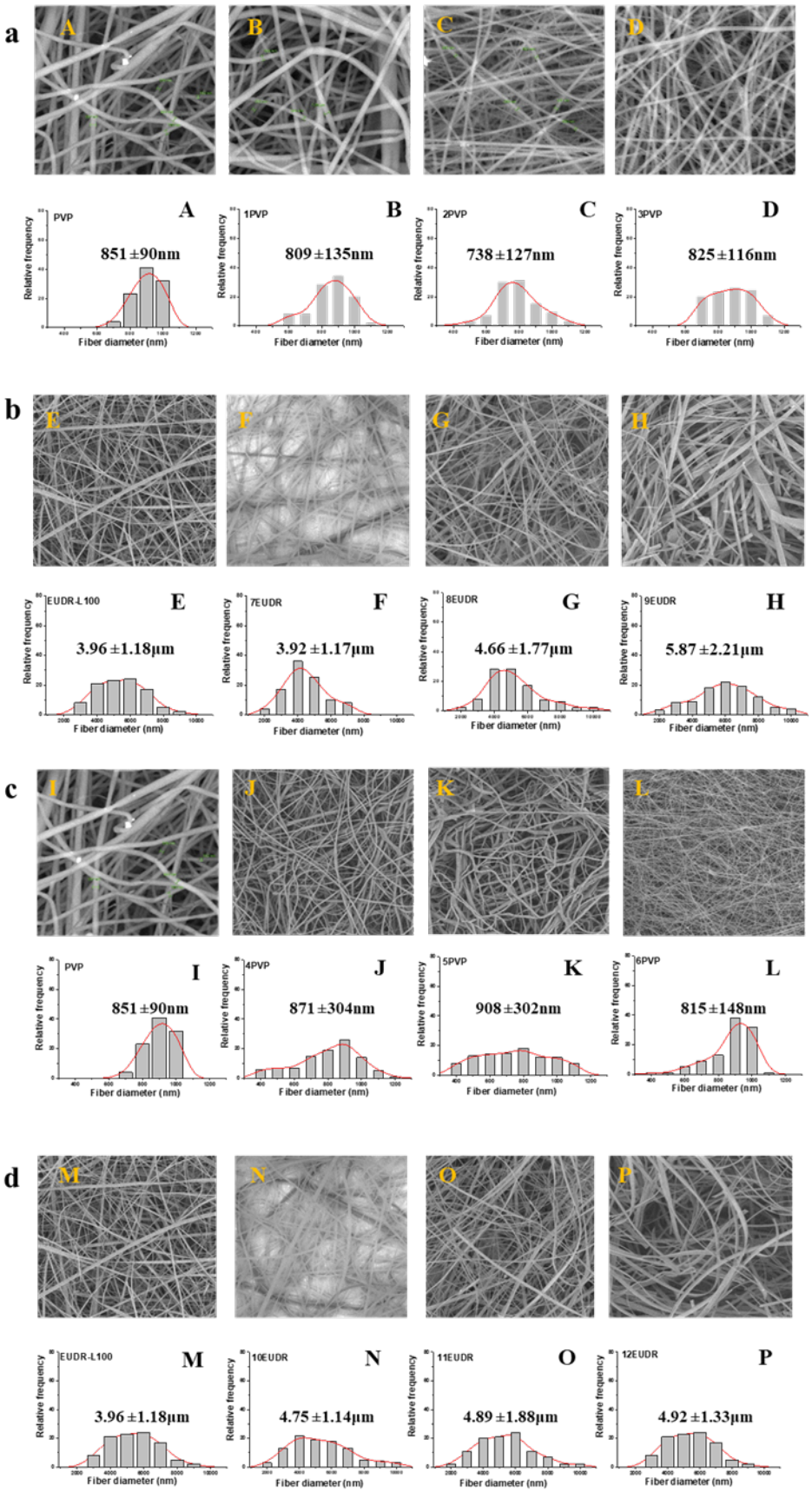
a
A
B
C
D
PVP
A
851±90nm
1PVP
B
809±135nm
2PVP
C
738±127nm
3PVP
D
825±116nm
Relative frequency
Fiber diameter (nm)
b
E
F
G
H
EUDR-L100
E
3.96±1.18μm
7EUDR
F
3.92±1.17μm
8EUDR
G
4.66±1.77μm
9EUDR
H
5.87±2.21μm
c
I
J
K
L
PVP
I
851±90nm
4PVP
J
871±304nm
5PVP
K
908±302nm
6PVP
L
815±148nm
d
M
N
O
P
EUDR-L100
M
3.96±1.18μm
10EUDR
N
4.75±1.14μm
11EUDR
O
4.89±1.88μm
12EUDR
P
4.92±1.33μm

FIGURE 2

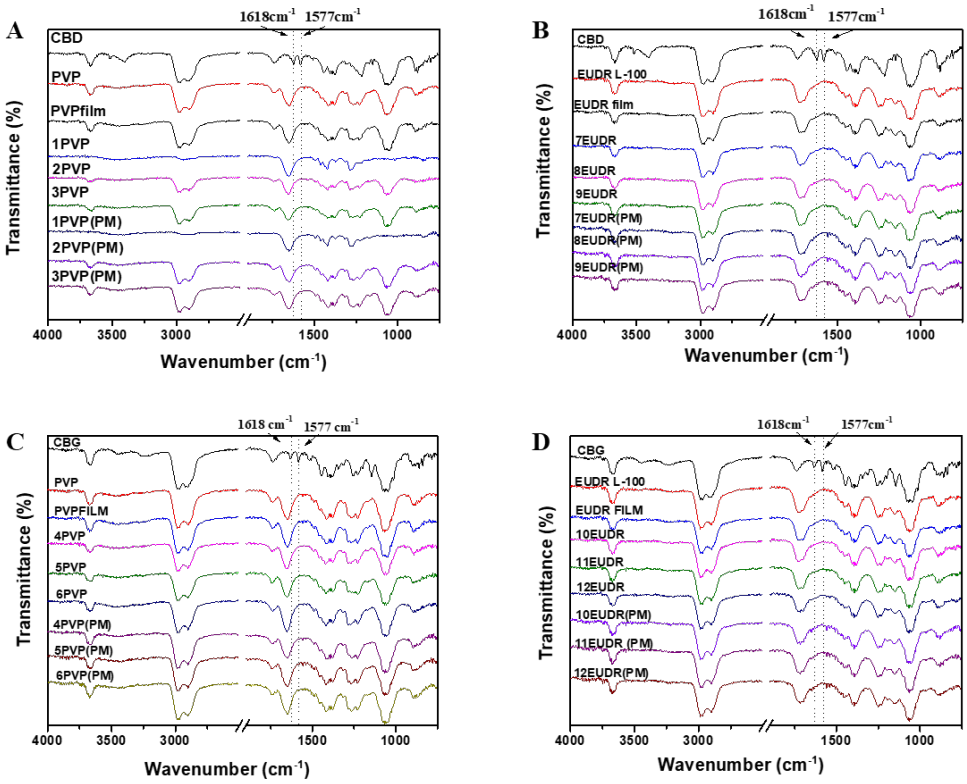
A
1618cm-1 1577cm-1
CBD
PVP
PVPfilm
1PVP
2PVP
3PVP
1PVP(PM)
2PVP(PM)
3PVP(PM)
Transmittance (%)
4000 3500 3000 1500 1000
Wavenumber (cm-1)
B
1618cm-1 1577cm-1
CBD
EUDR L-100
EUDR film
7EUDR
8EUDR
9EUDR
7EUDR(PM)
8EUDR(PM)
9EUDR(PM)
Transmittance (%)
4000 3500 3000 1500 1000
Wavenumber (cm-1)
C
1618 cm-1 1577 cm-1
CBG
PVP
PVPFILM
4PVP
5PVP
6PVP
4PVP(PM)
5PVP(PM)
6PVP(PM)
Transmittance (%)
4000 3500 3000 1500 1000
Wavenumber (cm-1)
D
1618cm-1 1577cm-1
CBG
EUDR L-100
EUDR FILM
10EUDR
11EUDR
12EUDR
10EUDR(PM)
11EUDR (PM)
12EUDR(PM)
Transmittance (%)
4000 3500 3000 1500 1000
Wavenumber (cm-1)

FIGURE 3

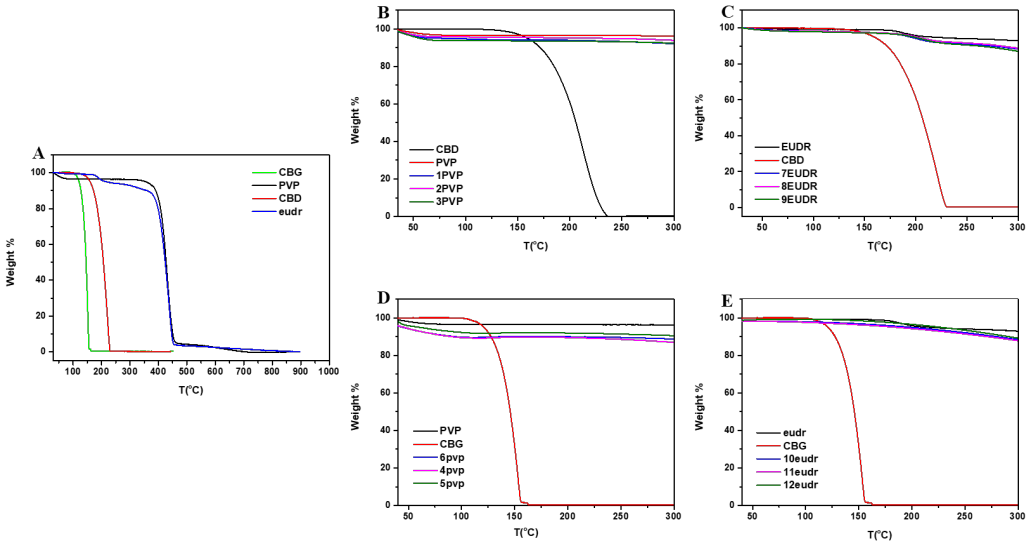
A
Weight %
T(°C)
CBG
PVP
CBD
eudr
B
Weight %
T(°C)
CBD
PVP
1PVP
2PVP
3PVP
C
Weight %
T(°C)
EUDR
CBD
7EUDR
8EUDR
9EUDR
D
Weight %
T(°C)
PVP
CBG
6pvp
4pvp
5pvp
E
Weight %
T(°C)
eudr
CBG
10eudr
11eudr
12eudr

FIGURE 4

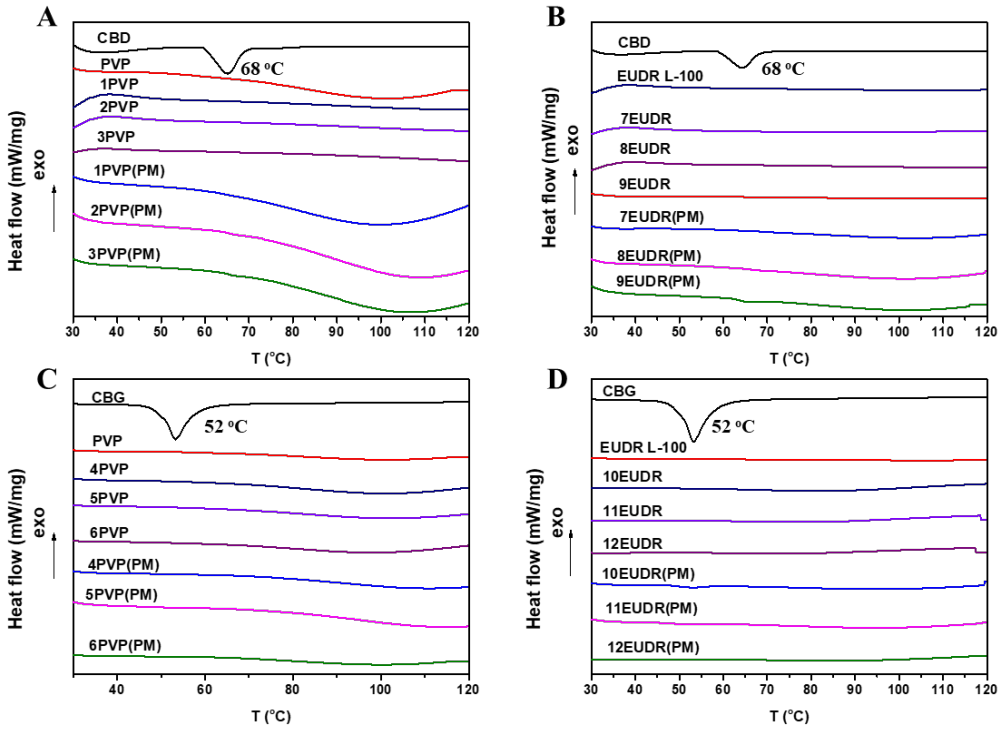
A
CBD
PVP
68 °C
1PVP
2PVP
3PVP
1PVP(PM)
2PVP(PM)
3PVP(PM)
Heat flow (mW/mg)
exo
T (°C)
B
CBD
EUDR L-100
68 °C
7EUDR
8EUDR
9EUDR
7EUDR(PM)
8EUDR(PM)
9EUDR(PM)
Heat flow (mW/mg)
exo
T (°C)
C
CBG
52 °C
PVP
4PVP
5PVP
6PVP
4PVP(PM)
5PVP(PM)
6PVP(PM)
Heat flow (mW/mg)
exo
T (°C)
D
CBG
52 °C
EUDR L-100
10EUDR
11EUDR
12EUDR
10EUDR(PM)
11EUDR(PM)
12EUDR(PM)
Heat flow (mW/mg)
exo
T (°C)

FIGURE 5

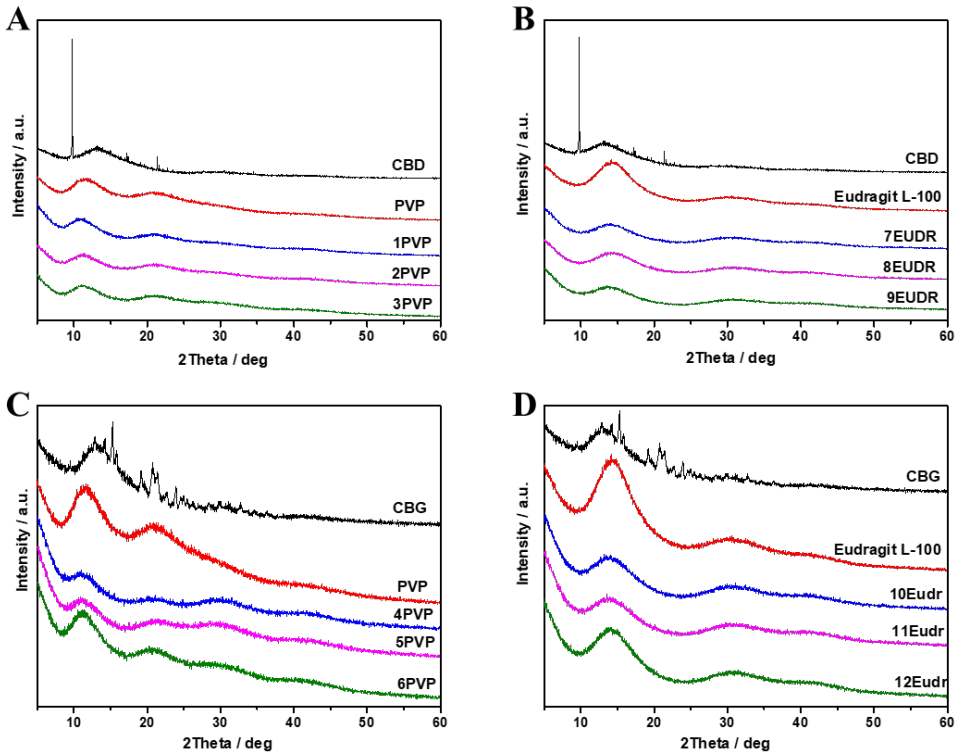
A
Intensity / a.u.
CBD
PVP
1PVP
2PVP
3PVP
10
20
30
40
50
60
2Theta / deg
B
Intensity / a.u.
CBD
Eudragit L-100
7EUDR
8EUDR
9EUDR
10
20
30
40
50
60
2Theta / deg
C
Intensity / a.u.
CBG
PVP
4PVP
5PVP
6PVP
10
20
30
40
50
60
2Theta / deg
D
Intensity / a.u.
CBG
Eudragit L-100
10Eudr
11Eudr
12Eudr
10
20
30
40
50
60
2Theta / deg

FIGURE 6

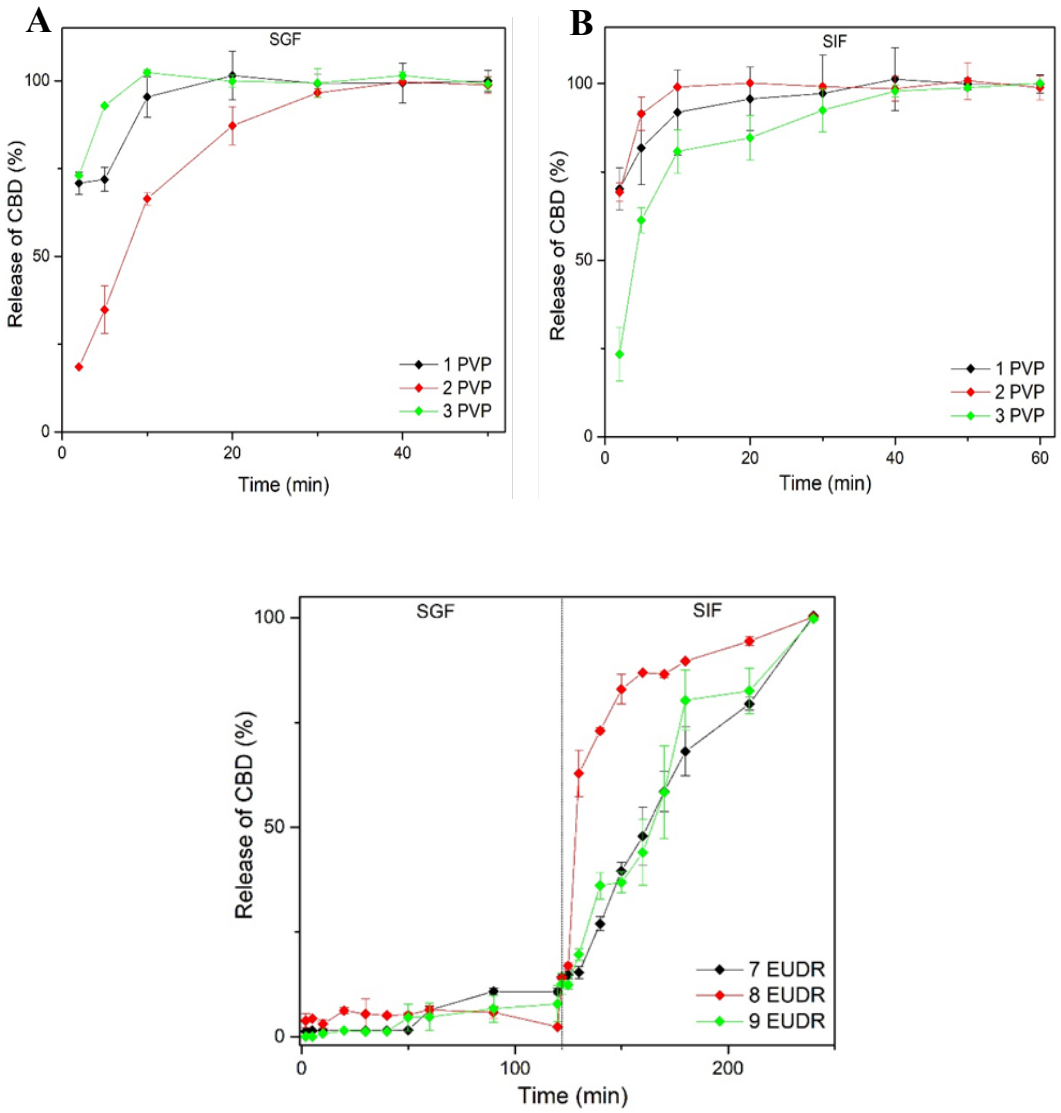
A
SGF
Release of CBD (%)
Time (min)
1 PVP
2 PVP
3 PVP
B
SIF
Release of CBD (%)
Time (min)
1 PVP
2 PVP
3 PVP
SGF
SIF
Release of CBD (%)
Time (min)
7 EUDR
8 EUDR
9 EUDR

FIGURE 7

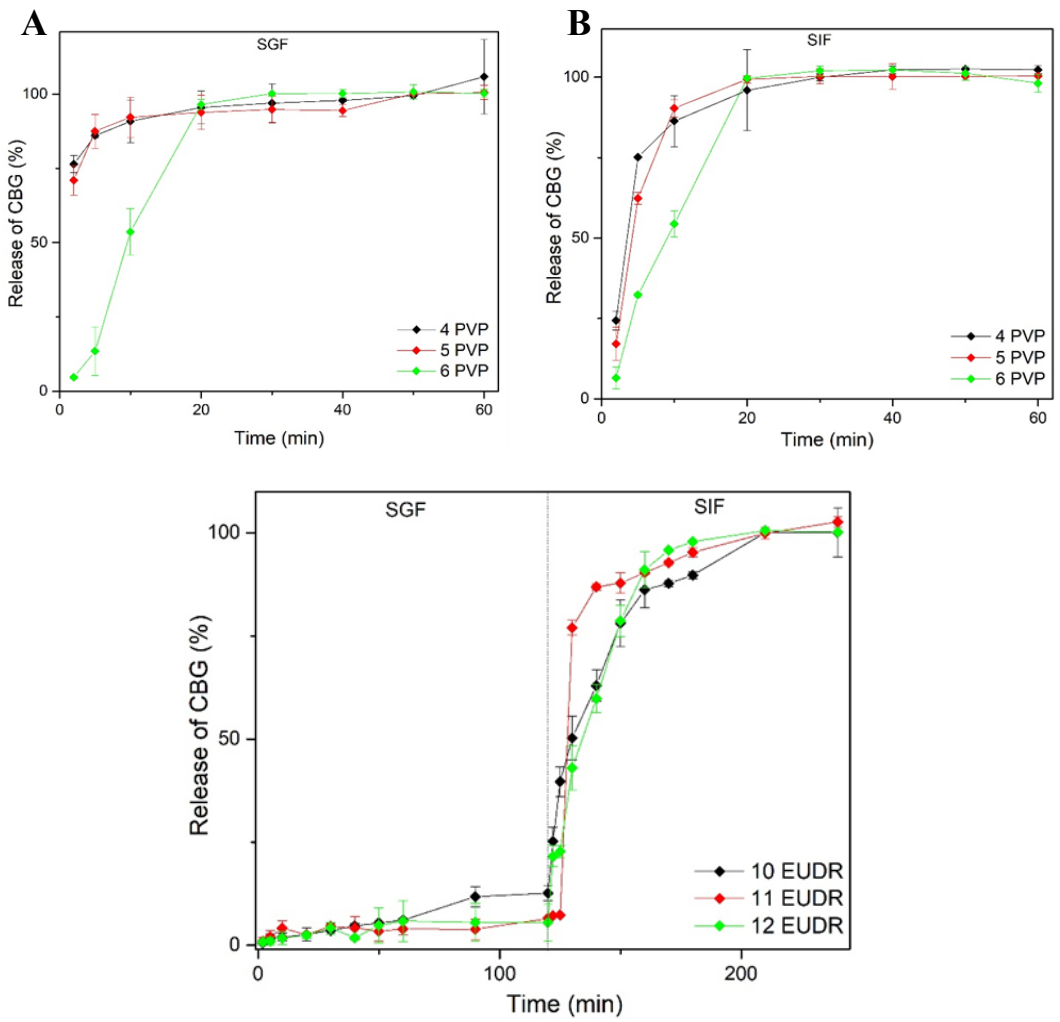
A
SGF
Release of CBG (%)
Time (min)
4 PVP
5 PVP
6 PVP
B
SIF
Release of CBG (%)
Time (min)
4 PVP
5 PVP
6 PVP
SGF
SIF
Release of CBG (%)
Time (min)
10 EUDR
11 EUDR
12 EUDR

907 **FIGURE 8**

908

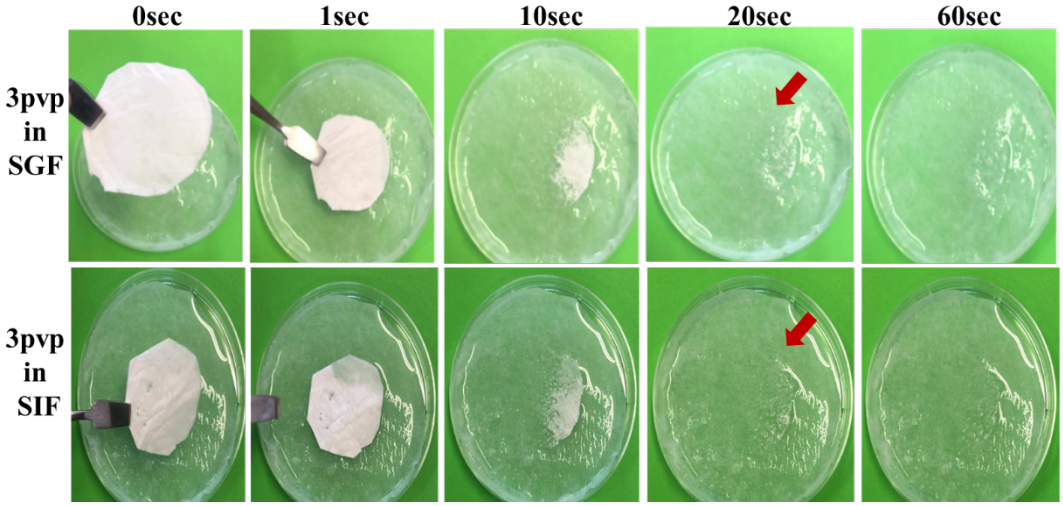

909

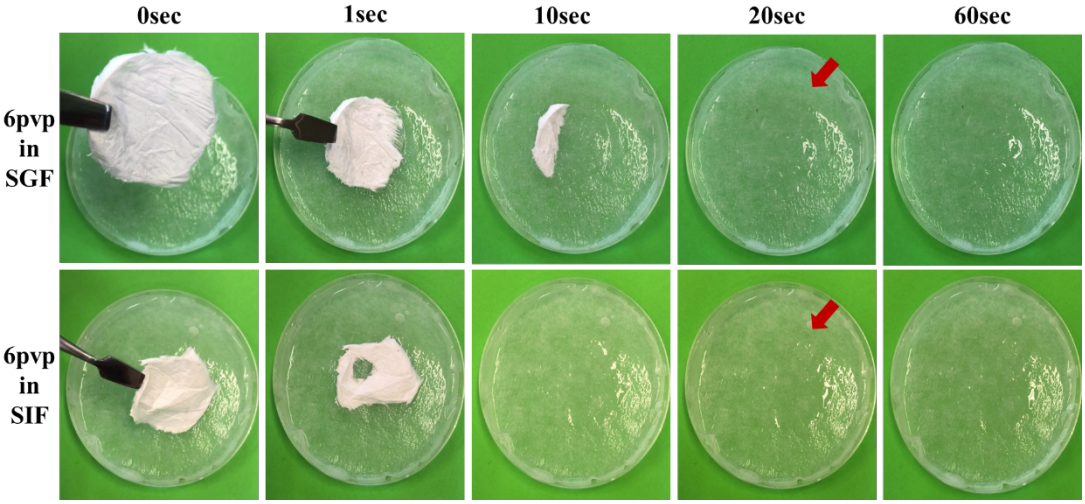

910

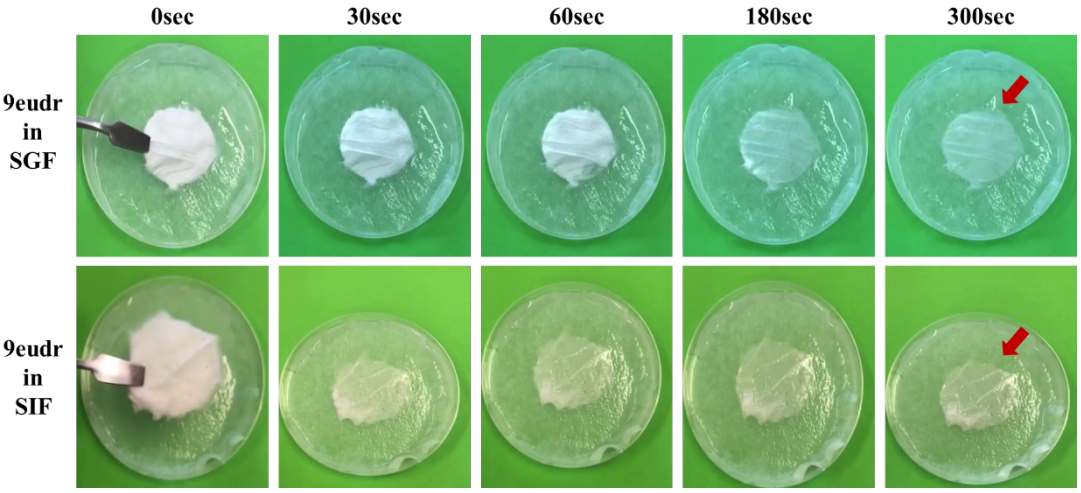

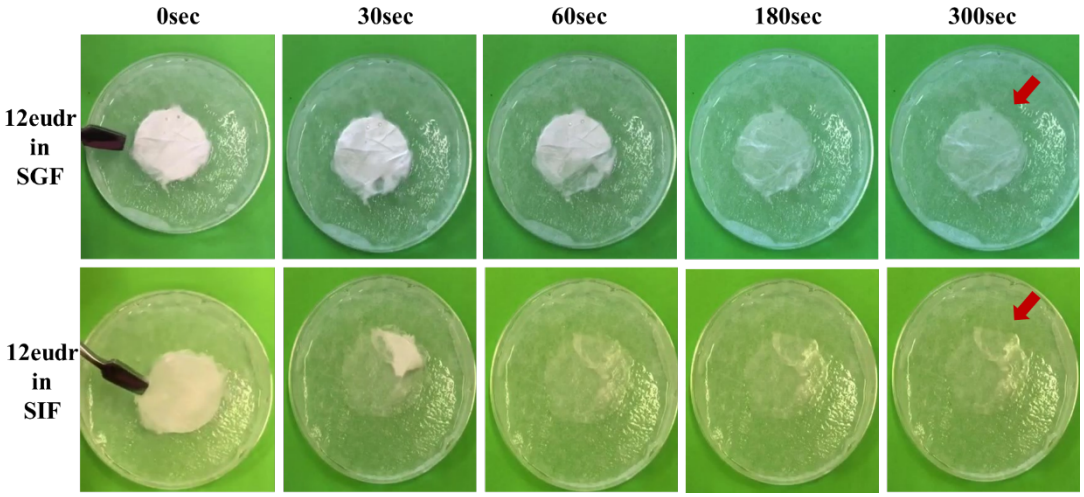
0sec
30sec
60sec
180sec
300sec
12eudr in SGF
12eudr in SIF

936 **FIGURE 9**

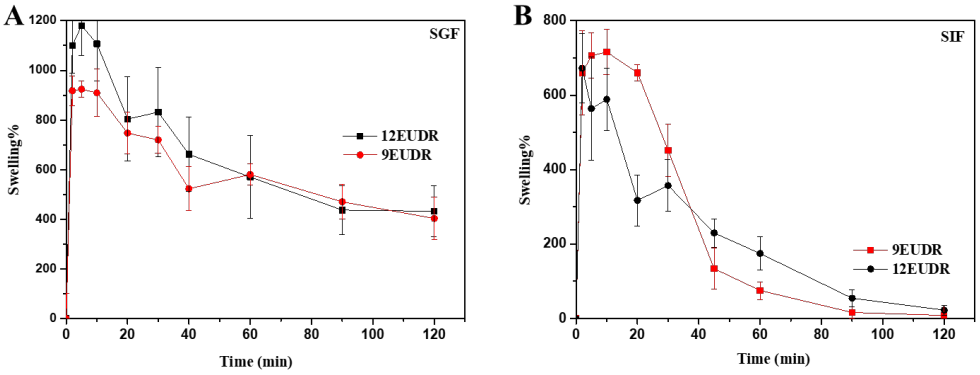

937